Scientia Iranica B (2018) 25(4), 2198–2207

Sharif University of Technology
Scientia Iranica
Transactions B: Mechanical Engineering
http://scientiairanica.sharif.edu

Two- and three-dimensional numerical simulations of supersonic ramped inlet

R. Askari and M.R. Soltani*

Department of Aerospace Engineering, Sharif University, Tehran, P.O. Box 1458889694, Iran.

Received 11 February 2017; received in revised form 8 May 2017; accepted 28 August 2017

KEYWORDS
Ramped inlet;
Supersonic;
External compression;
Numerical simulation;
Structural grid.

Abstract. Two-dimensional (2D) and three-dimensional (3D) numerical simulations of an external compression supersonic ramped inlet are presented for a free stream Mach number of 2. A comparison made between numerical results and experimental data showed that multi-block structured gird using standard $k-\varepsilon$ turbulence model gives acceptable results. The shape of present inlet diffuser was transformed gradually into a circular one to encompass the Aerodynamic Interface Plane (AIP). It was observed that the 3D simulation predicted a more accurate static pressure distribution during the length of supersonic inlet and total pressure distribution at the AIP in comparison with the 2D one. Further, a better estimation of Shock Boundary Layer Interaction (SBLI), shock structure, and turbulent flow was predicted by the 3D simulation. It appears that even though the 2D simulation scheme is widely used, it is a very weak method with low accuracy, while the 3D simulation is more accurate and gives a detailed flow field. Therefore, the 3D numerical simulation must be applied to the cases where a detailed flow study along with an accurate prediction of flow parameters as well as the shock structure is required.

1. Introduction

Air inlet is the first section of any aircraft propulsion system that provides sufficient airflow for the engine with minimum pressure loss under all flight conditions. This issue becomes more complicated for supersonic aircraft inlets due to wider ranges of flight Mach number, altitudes, angle of attack, etc. Supersonic inlet is designed to provide the required airflow with an acceptable level of energy (high pressure recovery) and quality (low distortion); further, it must have minimum drag, too [1,2].

Supersonic inlets are classified based on their various aspects such as region of supersonic flow compression (internal, external, or mixed compressions), flow structure dimensions (2D or ramped, axisymmetric, 3D or bumped, etc.), and position of installation (nose, side, ventral, top mounted, etc.) [3,4]. Depending on the maximum velocity of the vehicle, the supersonic compression is achieved in a multi-stage fashion, rather than a single-stage one, so that it can have a better performance. Multi-stage compression is fulfilled via double and multiple ramps or cones [3].

The shock waves formed on the external compression surfaces impinge at a point on the cowl lip, called impingement point. This condition is known as the Shock On Lip (SOL) condition, resulting in a maximum inlet mass flow and in a minimum spillage drag at the design point. In the real flight case, the aircraft experiences varieties of flight conditions where the impingement point might occur far from the cowl lip. In such situations, variable structures are utilized to adjust the inlet geometry to assure that the impinge-

*. *Corresponding author.*
E-mail address: msoltani@sarif.edu (M.R. Soltani)

doi: 10.24200/sci.2017.4495

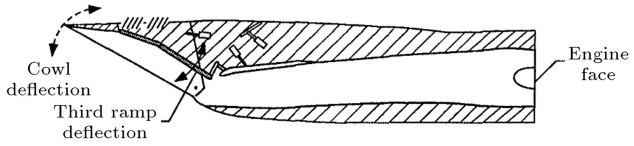

Figure 1. The F-15 variable geometry supersonic ramped inlet [6].

ment point will be located somewhere around the cowl lip. Therefore, the maximum mass flow and minimum spillage drag are achieved for all flight conditions [3,5]. These variable structures include variable ramps for 2D ramped inlet and an adjustable cone for axisymmetric or semi-axisymmetric inlets. Figure 1 shows a 2D variable structured supersonic ramped inlet of a fighter aircraft, F-15 [6].

The supersonic ramped inlet is one of the most common types of inlet due to its simplicity in design and analysis. The inlet is designed with multiple and variable structures for Mach numbers higher than one, which is expected for cruise condition to ensure the best performance in all flight conditions with which a vehicle may encounter during its flight [7]. It is a common practice to design and analyze this type of supersonic inlet two-dimensionally. Loth et al. [8] utilized a mesoflap flow control for a ramped inlet at a free stream Mach number of 2. They further tested this method of flow control for the same inlet equipped with a bleed system and compared both results with the solid surface (no-control) configuration. In addition, they performed a 2D numerical simulation using $k-\varepsilon$ turbulence model on an unstructured computational gird and compared the results with their experimental data. Ran and Mavris [9] provided a preliminary design method for a two-dimensional, mixed compression supersonic inlet to maximize total pressure recovery. They used a 2D numerical simulation to verify their results. Mizukami and Saunders [10] analyzed a rectangular, mixed-compression supersonic inlet using a 2D Navier-Stokes flow solver for various grids and turbulence models. They compared their numerical results with the experimental data and also with the original inviscid design data. They recommended a 2D Navier-Stokes code with $k-\varepsilon$ turbulence model as a useful tool for design and analysis of supersonic inlets. A 2D numerical simulation was performed by Chang et al. [11]. They used SST $k-\omega$ turbulence model and unsteady formulation to detect start/unstart phenomenon in a hypersonic inlet.

On the other hand, it should be considered that ramped inlet flows are significantly three-dimensional due to the sidewall effects (three-dimensional boundary layer thickening and the corresponding SBLI) and deformation of the stream-wise cross-sections in the diffuser geometry [12,13]. Therefore, in spite of high computational time and hardware costs, the 3D simulation provides detailed information about the flow field. Hence, there is a wide interest in 3D simulation of supersonic inlets flow field. Bourdeau et al. [14] developed and optimized a design method for high-speed inlets and verified their methodology with a 3D simulation case. They used a structured grid and $k-\varepsilon$ two-equation turbulence model. Aziz et al. [15] conducted a numerical study to establish an optimum design of a supersonic intake. Their flow simulation code solved time-dependent, Reynolds-averaged Navier-Stokes equations and used standard $k-\varepsilon$ model to simulate turbulent, compressible flow in a multi-zone structured grid. Trapier et al. [16] conducted a 3D numerical flow simulation of a ramped inlet using Delayed Detached Eddy Simulation (DDES), turbulence model with a structured computational gird using 20 million points to investigate the buzz phenomenon. They further verified their numerical results with the wind tunnel experimental data of Ref. [17].

Shock-wave Boundary Layer Interaction (SBLI) is one of the most important phenomenon that occurs in supersonic inlets, which will result in a very complicated flow structure, 3D phenomenon, and probable unsteadiness. SBLI occurs in all practical transonic, supersonic, and hypersonic vehicles [18]. In particular, Normal Shock-wave/Boundary-Layer Interaction (NSBLI) is a frequently occurring phenomenon that must be considered in supersonic inlet design[19]. Hamed and Shang reviewed and gathered a database for SBLI trend to predict flow patterns in supersonic inlets (their focus was on the mixed compression supersonic inlet). They further discussed the bleeding, suction, roughness, and blowing on the SBLI and its effects on the performance of supersonic inlets [20].

Despite vast 2D and 3D investigations by previous researchers, it is still unclear how to achieve the fastest and most accurate method to simulate the flow field of a 3D supersonic ramped inlet as well as its limitations. To fulfill the existing gap, the author conducted both 2D and 3D numerical simulations of an external compression supersonic ramped inlet introduced in [8]. The differences between 2D and 3D simulations are discussed thoroughly. It should be noted that the current study concerns supersonic ramped inlets only.

The most important parameters related to the inlet performance are Mass Flow Ratio (MFR), Pressure Recovery (PR), AIP Distortion Coefficient (DC), and inlet drag coefficient (Cd). Inlet Mass Flow Ratio (MFR) is the ratio of the actual inlet mass flow rate to the mass flow rate that an inlet can capture [21]. Pressure recovery is the ratio of the area-weighted averaged total pressure normalized by the free stream total pressure [8]. Aerodynamic Interface Plane, AIP, distortion is a measure of the non-uniformity of total pressure at that plane; however, there are various definitions for it depending on the engine specification, application, etc.

2. 2D numerical simulation of inlet flow field

Figure 2 illustrates the supersonic external compression ramped inlet used for the present numerical simulations. Loth et al. [8] tested this inlet in NASA Langley unitary plan wind tunnel, which is a closed-circuit, continuous-flow, variable density supersonic wind tunnel. Their experiments were conducted on a free stream Mach number of 2. As shown in Figure 2, this supersonic inlet has two compression ramped surfaces with 7 and 15 degrees' angles, respectively, that will compress the external flow with two relatively weak oblique shocks and a normal shock formed in front of the inlet entrance. This arrangement of shock waves is known as shock system or shock structure. The free stream supersonic Mach number decreases to a subsonic Mach number, i.e., 0.7 to 0.8, as the flow passes through this shock system. It then decreases further through subsonic diffuser to reach a Mach number of about 0.45 at the end of the diffuser, which is called Aerodynamic Interface Plane (AIP). AIP static pressure value is the main parameter that affects the inlet MFR due to both normal shock movement and deformation of shock structure. Hereafter, the Ramp compression surface and the Upper Diffuser Wall are named as RUDW and Cowl lip and the Lower Diffuser Wall as CLDW.

2.1. Numerical method, grid, and boundary condition considerations

The present simulations are conducted using the finite-volume method on a multi-block structured grid. The convection terms are treated using the second-order upwind implicit scheme in this study. In addition, turbulent kinetic energy and dissipation rate fluxes are discretized using first-order upwind schemes. The solutions continued until the energy and mass residuals decayed to values less than 10^{-4}. $k-\varepsilon$ turbulence model with the standard wall functions which is generally applicable to a wide range of flows and requires reasonable computational requirements [8,10], is employed. This turbulent model is favorable here due to its use in [8] and appears to give good results. The corresponding results provide a basis for verification of the present numerical simulations.

For 2D simulation, a structured grid with 110,000 cells is employed. The grid is clustered in the regions near the supersonic compression zone and cowl lip because of the presence of shock system, boundary layer thickening, and shock-boundary layer interaction. In addition, the grid clustering near the walls is used in the subsonic diffuser due to the possibility of boundary layer separation. Figure 3 shows the structured grid and flow boundary conditions used for the 2D simulation. Adiabatic, no-slip wall boundary condition is considered for ramp, cowl and diffuser. According to [8], the free stream Mach number is two and the AIP static pressure is 43.2 kPa for the design condition. The free stream stagnation pressure and temperature are 61.7 kPa and 339 K, respectively.

A grid resolution study using a finer grid was performed, confirming that the current grid is fine enough for the purposes of this study. The distribution of total pressure ratio at the AIP is plotted for various grid sizes in Figure 4. As seen from this figure, for grid sizes having more than about 110000 cells, there are no significant differences in the total pressure ratio distribution. Therefore, to have a balance between so-

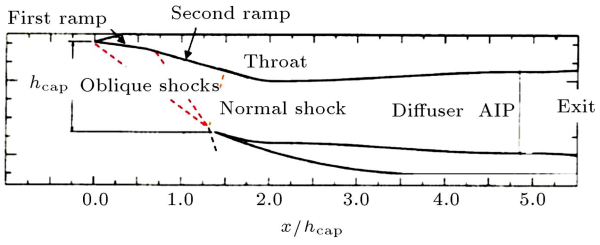

Figure 2. Geometry of supersonic external compression ramped inlet [8].

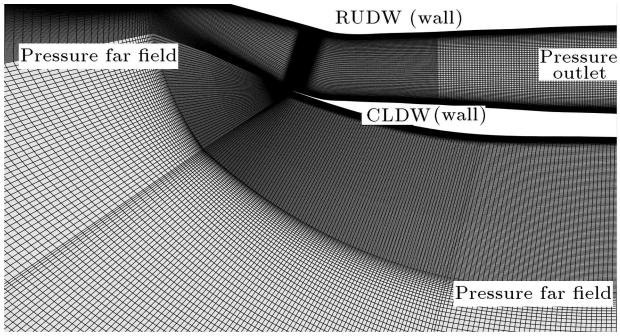

Figure 3. 2D grid and details of boundary conditions.

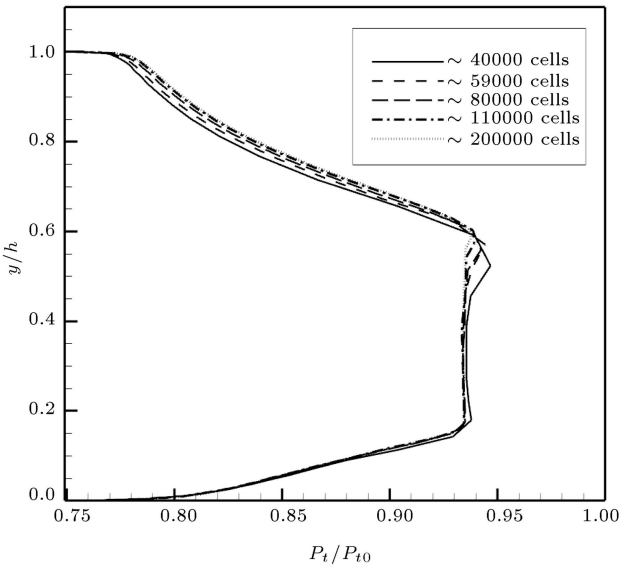

Figure 4. The distribution of total pressure ratio at the AIP for various grid sizes.

lution accuracy and computational cost, the grid with 110,000 cells is selected for the present 2D numerical simulations.

2.2. Results and discussions

Figure 5 presents the Mach number contour for this model. The first and second shock waves are seen to be impinging on the cowl lip as expected due to the supersonic compression ramps as well as the terminating normal shock. This phenomenon ensures that the intake operates at its maximum mass flow ratio while having minimum spillage drag. The supersonic flow Mach number decreases from 2 to 1.7 and, then, reduces to a value of 1.4 as it passes through the first and second oblique shocks, respectively. The flow becomes subsonic after it passes the normal shock, Mach $\approx$ 0.7 - 0.8, and its velocity decreases further until reaching the AIP location. Figure 6 shows the supersonic shock structure obtained from the present numerical simulation and is compared with the reports of [8]. As observed, the present 2D simulation results are compared very well with those reported by Loth et al. [8].

Figure 7 presents distributions of the ratio of the static pressure to the free stream total pressure on both RUDW and CLDW along the inlet and compares them with the experimental data of [8]. As observed, there is good agreement between the present numerical results and the experimental data of [8]. The static pressure jumps seen in this figure at two locations, $X/h_{\text{cap}} \approx 0.5$ and $X/h_{\text{cap}} \approx 1.4$, correspond to oblique and lambda shocks. The lambda shock pressure jump does not occur suddenly, because, at first, the flow passes through two weak oblique shocks (lambda shock feet), thus experiencing a gradual compression. For the sake of comparison with the experimental data, the criterion of SOL condition is considered as the best design condition. The 2D numerical simulations revealed that SOL condition would be satisfied at higher AIP pressure (about 7.64%), Figure 6. Consequently, as clearly seen from Figure 7, the diffuser static pressure distribution is higher than the experimental data of [8].

Figure 8 compares the present 2D numerical results of the total pressure ratio distribution at the AIP diameter with 2D numerical and experimental results of Ref. [8]. Y/h is the non-dimensional engine facing vertical position based on the AIP height (for 2D simulation) or diameter (for 3D simulation). This figure clearly shows that the present 2D simulation

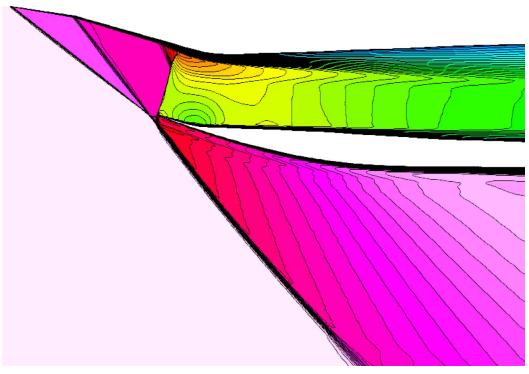

Figure 5. Contour of Mach number for 2D simulation.

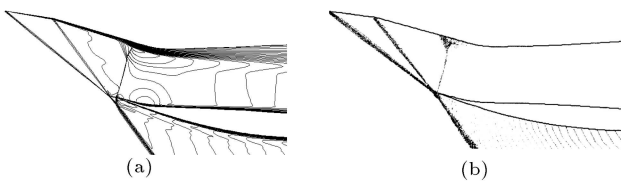

Figure 6. The contours of flow field Mach number for both present (a) and Loth's (b) [8] 2D simulation.

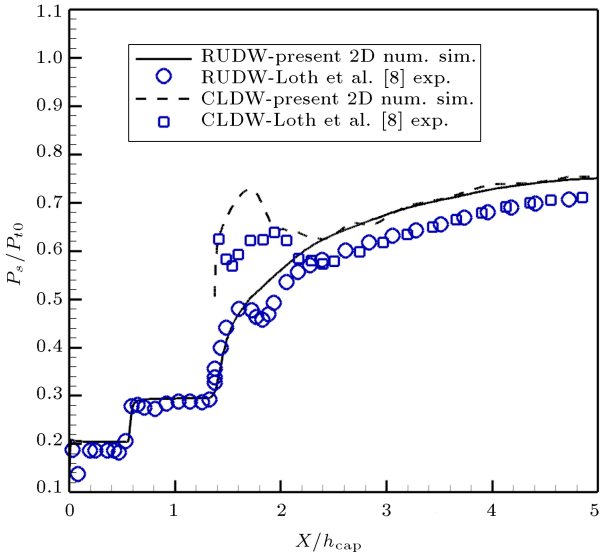

Figure 7. Distribution of the ratio of static pressure to free stream total pressure on the RUDW and CLDW.

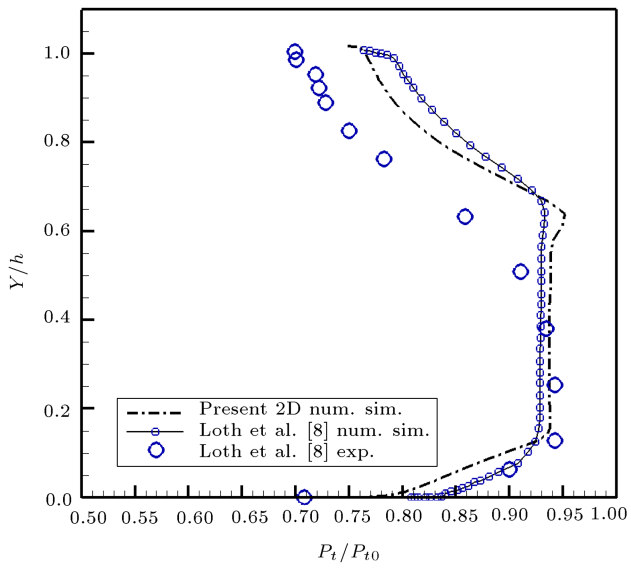

Figure 8. Total pressure ratio distribution at the AIP diameter.

results have good agreement with both 2D numerical results and experimental data of [8]. Further, it is observed that the present 2D simulation results are closer to the experimental data of [8] than their own 2D simulation data. It is further noted that both 2D simulation results, i.e., the present results as well as those of [8], predicted a wider uniform flow at the AIP when compared with the experimental data. Therefore, it is concluded that the 2D numerical simulation would result in a higher area weighed averaged total pressure, thus a higher PR is obtained at the AIP in comparison with the corresponding experimental results.

To study the differences between 2D numerical and experimental results, the flow field is divided into two regions. Generally, one can approximately distinguish between an outer-flow region (far from the surface boundary layer) as an inviscid and the region close to the surface as the viscous one, if assuming the shock wave as an inviscid phenomenon [22]; see Figure 9. Herein, the regions far from the RUDW and CLDW are called the *inviscid regions* where the flow experiences less viscous effects; the regions near the RUDW and CLDW are called the *viscous regions* where the shock wave interacts with the boundary layer and, consequently, the flow may separate into branches. Figure 8 indicates that the differences between the results of the present numerical simulations and the experimental ones are more prominent in the viscous regions, especially near the RUDW. Hence, it appears that the differences are due to the inaccurate prediction of 2D simulation results of SBLI on the compression ramp and in the turbulent flow downstream in the subsonic diffuser. The 2D numerical investigation predicted a weak lambda shock due to thin upstream boundary layer. It further did not predict any flow separation in the diffuser region where the flow is subsonic. These predictions would result in high levels of total pressure ratio at the AIP. However, Loth et al. [8] observed a thick ramp boundary layer and, consequently, a large lambda shock structure. They further reported flow separation in their experimental results, too. In Figure 8, the uniform total pressure portion in the AIP location originates from the upstream *inviscid regions*. There is a small jump in this uniform portion that is related to the part of the *inviscid* flow passing through the lambda shock feet. Further details are provided in Sections 3-4.

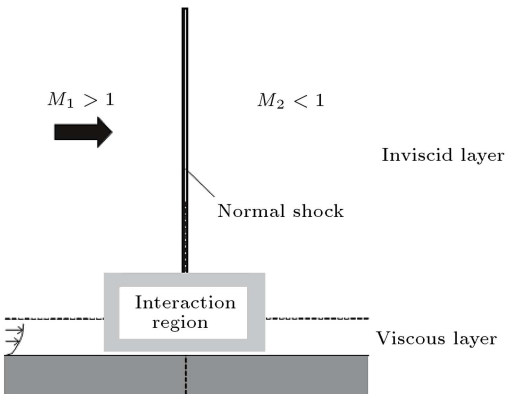

Figure 9. Schematic view of viscous and inviscid layers of fluid during formation of a normal SBLI.

There are several ways to achieve more accurate flow field simulation, including improvement of numerical method, increment of flow dimensions, and utilization of a more accurate turbulence model, to name a few. In the present study, increment of flow dimensions is considered and its effects will be investigated in detail. The reason is because the wind tunnel's experimental tests of [8] were conducted on a 3D geometry of a supersonic inlet, while the previous numerical simulations were limited to a 2D geometry of a supersonic inlet. Further, it is expected that a more accurate turbulent flow modeling would be obtained by a 3D simulation due to the 3D nature of the turbulent flow.

3. 3D numerical simulation of inlet flow field

As stated previously, in order to have a more comprehensive and accurate analysis of a supersonic inlet, 3D modelling and simulation are applied to have more consistency with the 3D geometry of the wind tunnel model. Figure 10 illustrates the 3D geometry of a semi-model of the present supersonic inlet along with the shape of the throat as well as several diffuser cross-sections. The cross-section in the region of compression ramp is obtained by extension of the 2D geometry in the third direction (z-axis). The shape of the cross-section is rectangular at the cowl lip (A-A) and at the throat (B-B) locations. From this section (B-B), the inlet shape then gradually morphs to a super elliptical shape in diffuser cross-sections C-C and D-D. Finally, it becomes circular at the AIP cross-section (close to E-E) where the inlet is connected to the engine face. Sidewalls are added to the 2D model in regions of the first and second compression ramps to isolate high-pressure flow of the compression region from the free stream one and further to force the supersonic flow over the ramp to become two-dimensional.

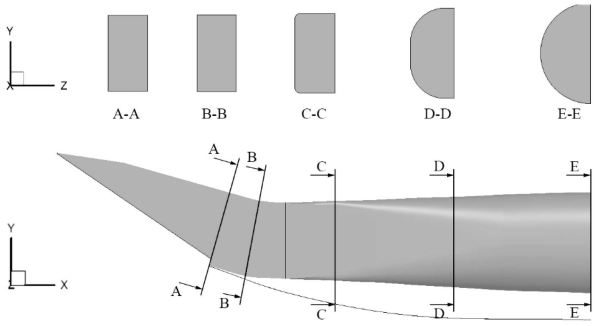

Figure 10. 3D geometry of supersonic inlet and its various sections.

3.1. Numerical method and grid considerations

The numerical method, boundary condition, and turbulence model used for the 3D simulation are the same as those used for the 2D case; see Subsection 2.1. Deriving benefit from the symmetry of geometry with respect to the xy-plane, a semi-model is utilized for the 3D simulation. A multi-block structured grid is generated for the 3D simulation. Grid is clustered into the supersonic compression regions near RUDW and CLDW to capture severe gradients of flow variables induced by the shock waves. This would facilitate an accurate prediction of shock system, shock-boundary layer interaction, and other phenomena that might be formed in this region. A grid resolution study was performed, and a computational grid containing at least 5,547,000 cells was shown to be adequate for the current study. In this computational grid, about 1.43 million cells are located in the supersonic regions (external compression ramp and free stream field), and about 1.48 million cells are located in the subsonic diffuser. Figure 11 shows the corresponding 3D grid along with further details for various views.

3.2. 3D simulation results

Figure 12 shows contour of Mach number on the xy-plane of symmetry for the present 3D simulation case. The oblique shocks are formed on the first and second ramps and terminate with a lambda shock wave in front of the cowl lip, as expected. Figure 13 illustrates 3D supersonic flow field's Mach number in the compression ramps, subsonic flow in the throat, and diffuser for various yz-planes. It is seen that the span-wise component of the flow velocity increases on the compression ramps in the stream-wise direction; thus, the flow becomes 3D, especially in the vicinity of the ramps, sidewalls, and cowl lip. This is in contrast to the expectation that the flow is 2D in the region of the compression ramps. This effect is more significant near the sidewalls. The flow in the subsonic diffuser is seen to be separated, forming a fully 3D vortical flow as it moves toward the AIP.

3.3. Verification and comparison of 2D and 3D simulations

Figure 14 presents distributions of the ratio of static pressure to free stream total pressure ratio on RUDW and CLDW with X/h_{cap} obtained from the present 2D and 3D numerical simulations' results and compares them with the experimental data of [8]. As observed, the 3D simulation' results have better agreement with the experimental data when compared with the 2D

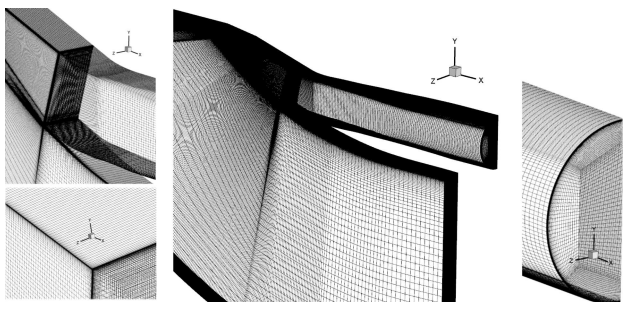

Figure 11. Multi-block structured 3D grid and details.

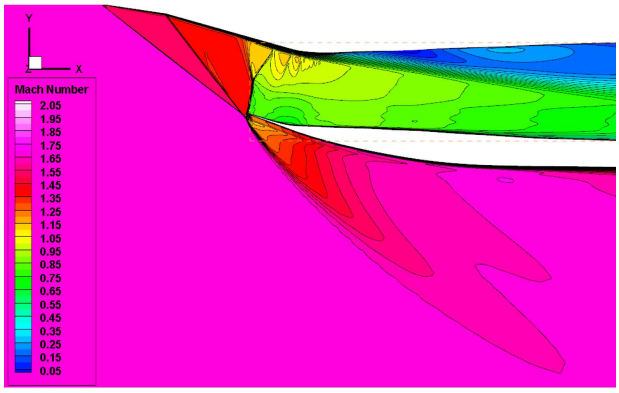

Figure 12. Contour of Mach number on the xy-plane of symmetry for the present 3D simulation.

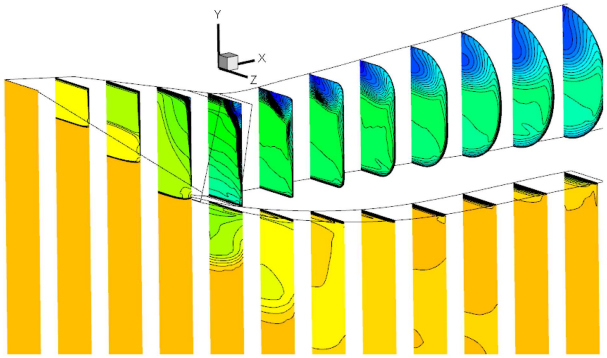

Figure 13. Contour of Mach number for various yz-planes for the present 3D simulation.

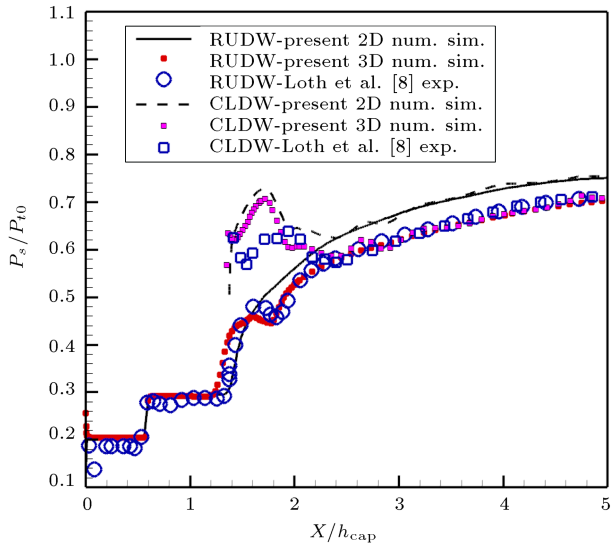

Figure 14. Distributions of static pressure to free stream total pressure ratio on the RUDW and CLDW.

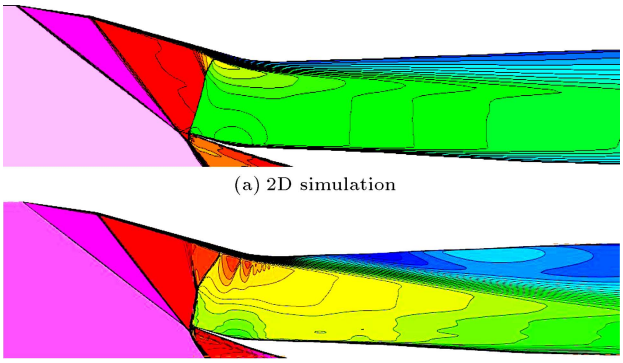

(a) 2D simulation

(b) 3D simulation

Figure 15. The contours of Mach number of the present 2D and 3D simulations on the xy-plane of symmetry.

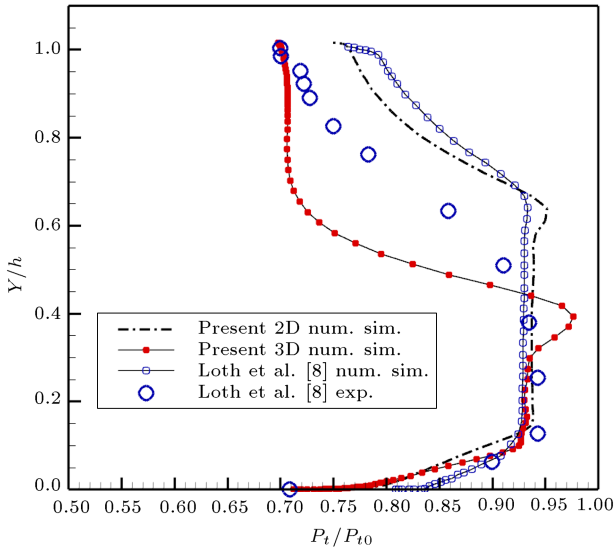

Figure 16. Total pressure ratio distributions at the AIP diameter for the present 2D and 3D simulations.

simulation case. The SOL condition for the 3D simulation is achieved for an AIP static pressure close to the test condition, while it is achieved in a higher AIP static pressure for the 2D simulation one. Thus, the diffuser pressure distribution for the 3D simulation, rather than with the previous 2D simulation, has much better agreement with the experimental data. To explain the differences better, contours of Mach numbers obtained from the present 2D and 3D simulations on the xy-plane of symmetry are plotted and compared in Figure 15. The differences are pronounced in the regions near the lambda shock and throat locations. Due to a stronger shock-boundary layer interaction in the 3D simulation case, the lambda shock is formed sooner and has a larger feet when compared with the one obtained for the 2D case. Therefore, a more gradual pressure rise associated with the lambda shock is evident in the 3D simulation result in comparison with the 2D one. In addition, the 3D flow faces a larger lambda shock feet and a thicker boundary layer. Under such circumstances, the width of *viscous region* increases which reduces the effective throat area. Furthermore, the 3D flow accelerates at the throat which decreases the static pressure slightly in this region. This reduction is evident from the static pressure ratio graph shown in Figure 14. The 3D flow separates on the RUDW surface due to the surface curvature in subsonic diffuser in the regions about $X/h_{\text{cap}} = 2.88$. This separated flow decelerates and its corresponding pressure rises until it reaches the AIP location, and the 3D vortical turbulent flow expands in the subsonic diffuser. However, there is no evidence of flow separation in the subsonic diffuser in the 2D simulation's results.

Figure 16 shows the total pressure ratio distribution at the AIP for the present 2D and 3D simulations' results and compares them with the 2D simulation and experimental data of Loth et al. [8]. The present 2D simulation predicted a wide region of uniform and high total pressure at the AIP diameter. However, the 3D simulation results show a larger turbulent region, hence a narrower region of high total pressure flow. The difference may be justified as follows. The 2D flow simulation is not able to predict the lambda shock strength and structure as well as the corresponding downstream turbulent flow accurately. However; the 3D simulation provides a better prediction for the SBLI, turbulent flow, and its span-wise flow extension because it considers a real 3D nature of supersonic and inlet flow and involves viscous effects related to the sidewalls and diffuser cross-sections [12]. Therefore, *viscous regions* in the 3D geometry increase, leading to a stronger SBLI in the supersonic compression, which affects downstream flow field in the regions of both throat and subsonic diffuser. This effect decreases the inlet capture area and, especially, throat effective area. As a result, the flow accelerates in the regions of throat in the 3D simulation case. In addition, the geometry of the diffuser transforms from rectangular shape at the throat location to a circular one at the AIP; thus, the flow is fully 3D in the subsonic diffuser. In contrast, in 2D modelling and flow simulation case, ramp sidewalls are ignored. Therefore, boundary layer growth in the span-wise direction is ignored in the 2D simulation study. Therefore, the diffuser sidewalls as well as the stream-wise deformation of diffuser test section are not considered in 2D simulation. As a result, the boundary layer growth and vortical separated region could not be simulated accurately.

Both 2D and 3D simulations provided relatively poor predictions of total pressure ratio in the portion of AIP diameter where the flow is turbulent. However, Figure 16 indicates that there are some advantages in the 3D simulation in comparison with the 2D case. The 3D simulation predicts the values of total pressure on both RUDW and CLDW very close to the experimental data, while the 2D simulation prediction is not accurate

enough. It seems that the reason for these differences is due to ignoring the ramps and diffuser sidewalls in the 2D simulation, while the 3D simulation case does not ignore them. In addition, the stream-wise deformation of diffuser sections can amplify these differences. These differences resulted in an accurate prediction of separation point for the 3D simulation case. As a result, a more accurate total pressure value on the RUDW and CLDW would be obtained in comparison with 2D simulation. Further, the uniform and high total pressure region predicted by the 3D simulation is more consistent with the experimental data of Ref. [8]. In other words, the 3D simulation provides a better prediction of the boundary between the two areas of uniform and non-unifrom (turbulent) flows. This advantage is most likely related to a more accurate prediction of SBLI and lambda shock structure in the 3D simulation since it considers ramps, sidewalls as well as their boundary layer growth. The differences in the portion of AIP diameter corresponding with the turbulent flow may be remedied by the implementation of a more accurate turbulence model, especially in the region of subsonic diffuser. This is, however, beyond the scope of the present study.

A jump in the total pressure ratio distribution is seen at the AIP for both 2D and 3D numerical simulations, as observed in Figure 16. This is due to the presence of the lambda shocks; note that the flow passing through these two oblique shock systems experiences lower total pressure loss in comparison when passing through a single normal shock one. As a result, there exists a region of high total pressure between the boundary-layer edge and slip surface. The width of this region is of the order of a few boundary-layer thicknesses [22]. Sometimes, this is considered as an advantage of the lambda shock system and is used in the supersonic flow field control to produce a high-level total pressure [23]. However, it is not desirable for the present application, since this region of high total pressure (which appears as a jump in Figure 15) can increase the flow distortion at the AIP, in spite of a slight increase in PR. To have a better insight, contours of total pressure are plotted along with the profiles of the total pressure distribution at the AIP for both present 2D and 3D numerical simulations in Figure 17.

The jump predicted by the 3D simulation is more significant in comparison with that predicted by the 2D simulation case. In other words, a region of higher total pressure in AIP appears in the 3D simulation results. By a careful examination of Figures 15 and 17, one can clearly see a region of secondary supersonic flow (supersonic tongue) after the lambda shock in the corresponding 3D simulation result, while such a supersonic tongue is not present in the contours of the 2D simulation one. It appears that a higher PR can be

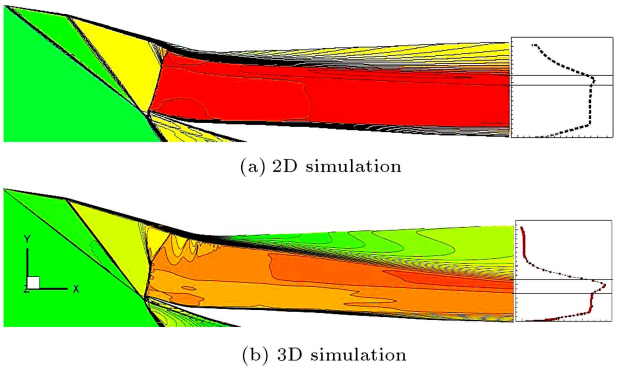

(a) 2D simulation

(b) 3D simulation

Figure 17. Contours of flow field total pressure besides the total pressure ratio distribution at the AIP for both present 2D (a) and 3D (b) numerical simulations.

achieved for the flow passing through multiple shocks related to lambda shock, and the following secondary supersonic region formed in the 3D simulation case is compared with the small lambda shock related to the 2D simulation one. This higher PR is responsible for the high total pressure jump at the AIP in the 3D simulation results.

Loth et al. [8] also mentioned the existence of a secondary region. They observed several features of the SBLI flow due to thickening of the boundary layer passing through the shock, which developed a significant "lambda foot". In addition, they reported several shock structures in the curved throat region, and mentioned that this flow feature usually shows signs of appreciable unsteadiness.

However, it is expressed that the boundary layer growth in the 3D geometry of a 2D ramped inlet due to SBLI on supersonic ramps and sidewalls is significant enough to affect the main flow properties due to the reduction of both effective capture and throat areas. Furthermore, 3D flow separation after normal shock and massive separation region in the diffuser are due to the 3D physics of flow, which occurs in a supersonic 2D ramped inlet.

4. Conclusion

Extensive 2D and 3D numerical simulations were conducted for an external compression supersonic ramped inlet. $k-\varepsilon$ turbulence model with the standard wall functions and structured grid was employed for both cases. The differences between 2D and 3D simulations were discussed thoroughly. The results showed that:

1. The distributions of static pressure to free stream total pressure ratio related to the 3D simulation on the RUDW and CLDW have better agreement with the experimental data. In addition, SOL condition is satisfied for the 2D simulation at higher AIP static pressure (about 7.64%) in comparison with

the 3D simulation as well as the experimental test condition;

2. It was observed that the span-wise component of the flow velocity increases on the compression ramp in the stream-wise direction, and the flow becomes 3D, especially near the ramp, sidewalls, and cowl lip. This is in contrast to the expectation that the flow is 2D in the region of the compression ramp. This effect is more pronounced near the sidewalls;
3. The 3D simulation predicts a separation point in the subsonic diffuser after the throat, while the 2D one does not predict any flow separation in the same region;
4. Both 2D and 3D simulations provide relatively poor predictions of total pressure ratio in the portion of AIP diameter which seems to be related to the presence of turbulent flow in this region. Total pressure ratio distribution at the AIP diameter indicates that the 3D simulation predicts the value of total pressure on both upper and lower walls very close to the experimental data, while the 2D simulation prediction is not accurate. Further, the region of uniform and high total pressure flow predicted by the 3D simulation is more consistent with the experimental data. The differences are more pronounced in the portion of AIP diameter which may be remedied by the implementation of a more accurate turbulence model, especially in the region of subsonic diffuser;
5. A jump in the total pressure distribution at the AIP is observed for both 2D and 3D numerical simulations and represents a high total pressure region. This is because the flow passing through lambda shocks experiences lower total pressure loss in comparison with the one passing through a single strong normal shock wave;
6. The 3D simulation predicts a region of supersonic tongue in the contour of Mach number after the lambda shock. The total pressure ratio related to the portion of internal flow passing from the lambda shock (and the following secondary supersonic region) is higher than the one passed from the normal shock;
7. Though the 2D simulation is widely used, it is a very weak and inaccurate tool, while the 3D simulation is more accurate and gives a detailed flow field. However, it is an expensive, yet high demanding tool for prediction and simulation of flow in the supersonic ramped inlet. In other words, the 3D numerical simulation must be applied for the cases where a detailed flow study and an accurate prediction of flow parameters as well as the shock structure are required.

In general, the boundary layer growth in 3D geometry of a 2D ramped inlet is significant enough to affect the main flow properties. The effects on the main flow are the results of reduction of both effective capture and throat areas in the 3D simulation case. In addition, 3D flow separation after normal shock and massive diffuser separation region are due to the 3D physics of flow, which occurs in supersonic 2D ramped inlet. The 2D simulation method could not predict any separation point for the present supersonic inlet. It seems that the 3D physics of flow is strongly effective, such that the 2D numerical simulation is not capable of capturing some phenomenon accurately, while acceptable detailed results can be obtained by the 3D flow simulation method.

Nomenclature

h	Height (m)
M	Mach number
P	Pressure (Pa)
X	X-axis (m)
Y	Y-axis (m)
Z	Z-axis (m)

Subscripts

0	Free stream
cap	Capture
d	Drag
s	Static condition
t	Total or stagnation condition

Abbreviations

2D	Two-dimensional
3D	Three-dimensional
AIP	Aerodynamic Interface Plane
C	Coefficient
DC	Distortion Coefficient
CLDW	Cowl lip and Lower Diffuser Wall
MFR	Mass Flow Ratio
NSBLI	Normal Shock Boundary Layer Interaction
SBLI	Shock Boundary Layer Interaction
RUDW	Ramp compression surface and Upper Diffuser Wall

References

1. Mattingly, J.D. and Von Ohain, H. "Elements of propulsion: gas turbines and rockets", *American Institute of Aeronautics and Astronautics Reston*, Va, USA (2006).
2. Soltani, M.R. and Sepahi-Younsi, J. "Buzz cycle de-

scription in an axisymmetric mixed-compression air intake", *AIAA Journal*, **54**(3), pp. 1040-1053 (2015).

3. Seddon, J.M. and Goldsmith, E., *Intake Aerodynamics*, Blackwell Science, Ebook (1999).
4. Soltani, M.R., Daliri, A., and Sepahi Younsi, J. "Effects of shock wave/boundary-layer interaction on performance and stability of a mixed-compression inlet", *Scientia Iranica. Transaction B, Mechanical Engineering*, **23**(4), p. 1811 (2016).
5. Goldsmith, E.L. and Seddon, J., *Practical Intake Aerodynamic Design*, Amer Inst of Aeronautics (1993).
6. Orme, J.S. and Conners, T.R. "Supersonic flight test results of a performance seeking control algorithm on a NASA F-15 aircraft", *AIAA Paper*, pp. 1994-3210 (1994).
7. Whitford, R., *Design for Air Combat*, Janes Information Group (1987).
8. Loth, E., Jaiman, R., Dutton, C., and White, S. "Mesoflap and bleed flow control for a Mach 2 inlet", *AIAA Paper*, pp. 2004-855 (2004).
9. Ran, H. and Mavris, D. "Preliminary design of a 2D supersonic inlet to maximize total pressure recovery", in *AIAA 5th Aviation, Technology, Integration and Operations Conference*, Virginia, pp. 2005-7357 (2005).
10. Mizukami, M. and Saunders, J. "Parametrics on 2D Navier-Stokes analysis of a Mach 2.68 bifurcated rectangular mixed-compression inlet", *31st Joint Propulsion Conference and Exhibit* (1995).
11. Chang, J., Hu, Q., Yu, D., and Bao, W. "Classifier utility modeling and analysis of hypersonic inlet start/unstart considering training data costs", *Acta Astronautica*, **69**(9), pp. 841-847 (2011).
12. Loth, E., Titchener, N., Babinsky, H., and Povinelli, L. "Canonical normal shock wave/boundary-layer interaction flows relevant to external compression inlets", *AIAA Journal*, **51**(9), pp. 2208-2217 (2013).
13. Fisher, S. "Three-dimensional flow effects in a two-dimensional supersonic air intake", *Journal of Propulsion and Power*, **2**(6), pp. 546-551 (1986).
14. Bourdeau, C., Carrier, G., Knight, D., and Rasheed, K. "Three dimensional optimization of supersonic inlets", *AIAA Paper*, pp. 1999-2108 (1999).
15. Aziz, M.A., Elbanna, H.M., and Abdelrahman, M.M. "Design and optimization of a three dimensional supersonic intake using the CFD-RC package", In *Tenth International Congress of Fluid Dynamics* (2010).
16. Trapier, S., Deck, S., and Duveau, P. "Delayed detached-eddy simulation of supersonic inlet buzz", in *Advances in Hybrid RANS-LES Modelling*, Springer, pp. 242-251 (2008).
17. Trapier, S., Duveau, P., and Deck, S. "Experimental study of supersonic inlet buzz", *AIAA Journal*, **44**(10), pp. 2354-2365 (2006).
18. Gaitonde, D.V. "Progress in shock wave/boundary layer interactions", *Progress in Aerospace Sciences*, **72**, pp. 80-99 (2015).
19. Jaiman, R.K., Loth, E., and Dutton, J. "Simulations of normal shock-wave/boundary-layer interaction control using mesoflaps", *Journal of Propulsion and Power*, **20**(2), pp. 344-352 (2004).
20. Hamed, A. and Shang, J. "Survey of validation data base for shockwave boundary-layer interactions in supersonic inlets", *Journal of Propulsion and Power*, pp. 1991-617-625 (1991).
21. Soltani, M.R., Younsi, J.S., Farahani, M., and Masoud, A. "Numerical simulation and parametric study of a supersonic intake", *Proceedings of the Institution of Mechanical Engineers, Part G: Journal of Aerospace Engineering*, **227**(3), pp. 467-479 (2013).
22. Babinsky, H. and Harvey, J.K., *Shock Wave-Boundary-Layer Interactions*, **32**, Cambridge University Press (2011).
23. Ogawa, H. and Babinsky, H. "Shock/boundary-layer interaction control using three-dimensional bumps in supersonic engine inlets", in *AIAA Paper 46th Aerospace Sciences Meeting and Exhibit* (2008).

Biographies

Rasoul Askari was born in Isfahan, Iran in 1985. He received his MS degree in Propulsion from Aerospace Engineering Department in Sharif University of Technology, Tehran, Iran. He is currently a PhD candidate in the propulsion in Sharif University of Technology at the Department of Aerospace Engineering. His fields of interest are applied numerical and experimental aerodynamics and propulsion.

Mohammad Reza Soltani received his PhD degree in Aerodynamics from the University of Illinois at Urbana-Champaign, USA, and is now a Professor at the Aerospace Engineering Department in Sharif University of Technology, Tehran. His research interests include applied aerodynamics, unsteady aerodynamics, wind tunnel testing, wind tunnel design, and data processing.